

Formation of various TiO₂ nanostructures from electrochemically anodized titanium

Jun Wang,^a Lei Zhao,^a Victor S.-Y. Lin^b and Zhiqun Lin^{*a}

Received 3rd March 2009, Accepted 14th March 2009

First published as an Advance Article on the web 20th April 2009

DOI: 10.1039/b904247d

TiO₂ nanostructures, including nanowires, highly ordered nanotube arrays, and single crystalline nanoplates, were obtained from electrochemically anodized Ti foil in a fluorine-containing ethylene glycol electrolyte. The TiO₂ nanowires, formed by the electric field induced chemical splitting of TiO₂ nanotubes by fluoride ions during a lengthy anodization can be isolated from the nanotube arrays by mild ultrasonication. The highly ordered TiO₂ nanotubes buried underneath are thus exposed. The transformation of as-prepared amorphous TiO₂ nanotubes into the anatase or rutile phase as a function of annealing temperature was systematically scrutinized by Raman spectroscopic measurements in conjunction with TEM imaging. In the latter study, the ultramicrotomed sections of the samples clearly exhibited the formation of highly crystalline TiO₂. More importantly, crystalline TiO₂ nanotubes were mechanically broken into intriguing single crystalline TiO₂ nanoplates as a result of ultramicrotoming. The present study not only demonstrates a facile approach to produce high quality TiO₂ nanowires, nanotubes, and nanoplates in a simple manner, but also provides valuable insights into temperature dependent crystalline transformation in the anodic TiO₂ nanotube arrays.

Introduction

Wide band gap semiconductor titania, also known as titanium(IV) dioxide, TiO₂, is a very useful functional material. TiO₂ exists mainly in three forms in nature: rutile, anatase, and brookite, with two additional high pressure phases: the monoclinic baddeleyite and an orthorhombic PbO₂-like phase.¹ Compared to the bulk counterparts, TiO₂ nanostructures with controlled dimensions, including nanoparticles, nanowires, nanotubes, and mesoporous films, possess much larger surface area to volume ratios, thereby providing additional reactive sites for catalyzing, sensing, and miscibility with other materials. They exhibit promising performance and have been widely exploited for use in the areas of gas sensors,^{2–4} hydrogen generation,^{5,6} photocatalysts,^{7,8} cell separation,⁹ dye sensitized solar cells (DSSC),^{10–19} and quantum dot^{20–26} sensitized solar cells.²⁷ In the latter context, rather than sintered TiO₂ nanoparticle films in which electrons hop between nanoparticles,^{19,28} self-organized TiO₂ nanotube arrays provide a direct pathway for efficient electron transport from interface to electrode. These TiO₂ nanotube arrays are prepared by electrochemical anodization of Ti in a fluorine-containing electrolyte and employed as the photoanode, where each individual TiO₂ nanotube is perpendicular to the membrane surface.^{16,29–31}

Since the as-prepared anodic TiO₂ nanotube arrays are amorphous, high temperature annealing is necessary to convert them into crystalline forms for high performance applications. However, to the best of our knowledge, little work has been done on the systematic study of temperature dependent crystalline evolution in anodic TiO₂ nanotube arrays.^{32,33} Herein, we

described the fabrication of various TiO₂ nanostructures, including nanowires, highly ordered nanotube arrays, and single crystalline nanoplates, from electrochemically anodized Ti foil. The TiO₂ nanowires, which were formed due to the electric field induced chemical splitting of TiO₂ nanotubes by fluoride ions upon lengthy anodization, can be isolated from the nanotube arrays by mild ultrasonication. The highly ordered TiO₂ nanotube arrays buried underneath are thus exposed. The transformation of as-prepared amorphous TiO₂ nanotubes into the anatase or rutile phase as a function of annealing temperature was systematically scrutinized by Raman spectroscopic measurements in conjunction with TEM imaging. In the latter study, the ultramicrotomed sections of samples clearly exhibited the formation of highly crystalline TiO₂. More importantly, crystalline TiO₂ nanotubes were mechanically broken into intriguing single crystalline TiO₂ nanoplates as a result of ultramicrotoming.

Experimental

Fabrication of freestanding TiO₂ nanotube arrays

Freestanding TiO₂ nanotube arrays were prepared using a previously reported approach,³⁴ which includes two steps, namely, the synthesis of TiO₂ nanotube arrays with a high length/diameter aspect ratio on highly pure Ti foil, followed by detachment of nanotube arrays from the metallic Ti substrate. Briefly, Ti foil (Sigma-Aldrich; 250 μm thick, 99.7% purity) was degreased by ultrasonication for 30 min in a mixture of acetone, methanol, and methylene chloride, followed by a thorough rinse with DI water and blow dried with N₂ gas. Ethylene glycol (Fisher Scientific) was used as the electrolyte in which a small amount of ammonium fluoride (Sigma-Aldrich) was added. Ti foil was electrochemically anodized at a constant potential of

^aDepartment of Materials Science and Engineering, Iowa State University, Ames, IA, 50011, USA. E-mail: zqlin@iastate.edu

^bDepartment of Chemistry, Iowa State University, Ames, IA, 50011, USA

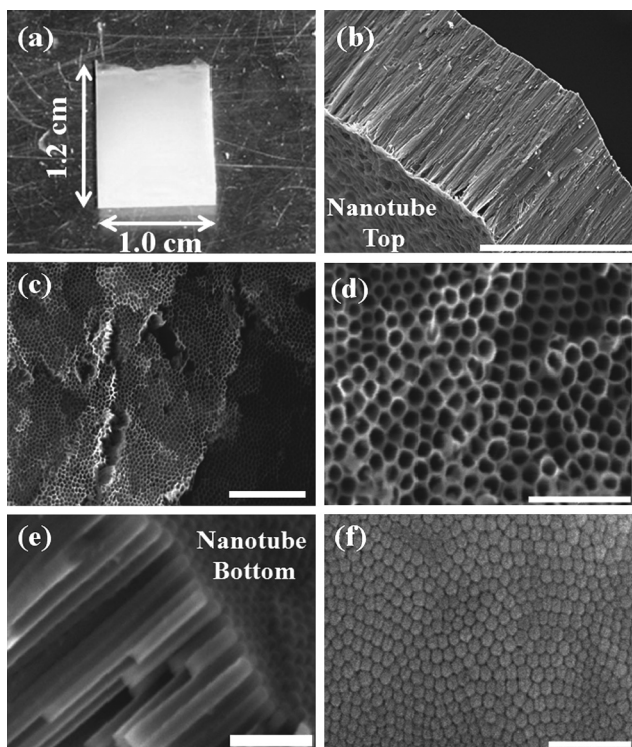


Fig. 1 (a) Digital image of a freestanding TiO_2 nanotube membrane. The lateral dimension is $1.2 \times 1.0 \text{ cm}^2$. (b) SEM image of as-prepared freestanding TiO_2 nanotube arrays (cross sectional view, scale bar = $50 \mu\text{m}$). (c–f) SEM images of the freestanding TiO_2 nanotube arrays after mild ultrasonication: (c) low magnification (scale bar = $2 \mu\text{m}$) and (d) high magnification SEM images (scale bar = $1 \mu\text{m}$) (top view); (e) cross-sectional view (scale bar = $1 \mu\text{m}$); and (f) bottom view (scale bar = $1 \mu\text{m}$).

60 V for a long period of time (*e.g.*, 60 h in the present study) in a two-electrode cell at room temperature using a power source EC570-90 (Thermo Electron Corporation), in which a platinum foil was used as the counter electrode. After anodization, the Ti foil with the TiO_2 nanotubes grown on one side of its surfaces was extensively washed with DI water and methanol and kept in a methanol bath overnight. Then, the anodized Ti foil was taken out from the methanol bath and washed again with a large amount of methanol, and the foil was placed at the bottom of a large chamber with the anodized surface facing up. The evaporation of methanol caused the light yellowish membrane to gradually separate from the Ti substrate (Fig. 1a) as a result of surface tension-driven delamination of the TiO_2 barrier layer (*i.e.*, a thin layer formed between the TiO_2 nanotube array and the Ti foil during anodization) owing to the presence of methanol in the defect areas of the barrier layer.³⁴

Formation of TiO_2 nanowires *via* ultrasonication

Close examination of freestanding TiO_2 nanotubes right after separation from the Ti foil revealed that a layer of TiO_2 nanowires covered their top (Fig. 2). Mild ultrasonication of the membrane in methanol was thus conducted for a few minutes, during which a very thin layer on top of the membrane was gradually broken and dispersed into the methanol, thereby

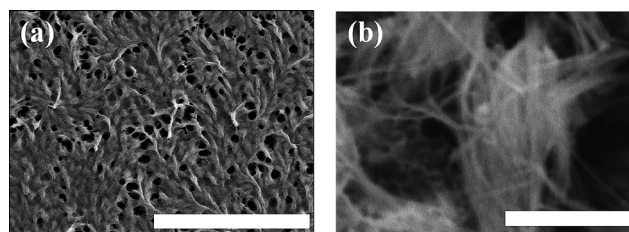


Fig. 2 SEM images of TiO_2 nanowires obtained from the splitting of electrochemically anodized TiO_2 nanotubes upon lengthy anodization. (a) Low magnification, scale bar = $50 \mu\text{m}$, and (b) high magnification, scale bar = 500 nm .

exposing the underlying TiO_2 nanotubes in the membrane. This very thin layer was examined by SEM (Fig. 2).

Crystallization of TiO_2 nanotube arrays

The as-prepared freestanding amorphous TiO_2 nanotube arrays were transformed into the anatase or rutile crystalline phase after annealing in air for 3 h at different temperatures, ranging from $200 \text{ }^\circ\text{C}$ to $800 \text{ }^\circ\text{C}$.

Formation of TiO_2 nanoplates *via* ultramicrotome

Freestanding TiO_2 nanotube arrays annealed at different temperatures were embedded in Spurr's resin, followed by curing at $60 \text{ }^\circ\text{C}$ for 48 h. Ultramicrotoming of the embedded TiO_2 nanotubes was performed on a Leica Reichert Ultracut using a freshly made glass knife. Thin sections with a thickness of 70 nm were collected on carbon coated copper grids (400 mesh) for TEM characterization. For comparison, thin sections of amorphous TiO_2 nanotube arrays were also prepared. The TEM sample preparation method was maintained the same for all annealed samples.

Characterization

SEM imaging was carried out on a JEOL 5800 LV scanning electron microscope (SEM) at a 15 kV accelerating voltage. Specifically, mechanically broken TiO_2 nanotube arrays were mounted on conductive carbon tapes, which were then attached to the surface of SEM brass stubs. The samples were coated with a thin layer of Au/Pd by sputtering to minimize the charging effect under the SEM imaging condition. TEM and high resolution TEM (HRTEM) were performed on a JEOL 2100 scanning transmission electron microscope (STEM), operated at 200 kV. Confocal Raman measurements were conducted on a Renishaw inVia Raman microscope excited with a 488 nm Ar⁺ laser at 5 mW with a 10 s acquisition time.

Results and discussion

1. TiO_2 nanowires and nanotubes

Freestanding TiO_2 nanotube arrays were first fabricated according to our previously reported mechanical delamination approach.^{34,35} The evaporation of methanol caused the yellowish membrane to detach from the metallic Ti foil as a result of surface tension-driven delamination of the TiO_2 barrier layer

that was formed between the TiO₂ nanotube arrays and the Ti foil during anodization (see Experimental section). A digital image of a freestanding TiO₂ membrane with lateral dimensions of 1.2 × 1.0 cm² is shown in Fig. 1a. Close examination of the freestanding TiO₂ membrane revealed that the surface of the membrane was covered by a layer of TiO₂ nanowires (Fig. 1b and 2). The thickness of the nanowire layer was ~100 nm as measured by SEM. The formation of a thin layer of TiO₂ nanowires was attributed to electric field induced chemical etching of TiO₂ nanotubes in a “bamboo-splitting” mode, that is, anodically grown nanotubes vertically split upon a long period of anodization.^{36,37} The nanowires can be successfully isolated by mild ultrasonication (Fig. 2), thereby exposing the nanotube arrays buried beneath. Removal of these nanowires is necessary for the application of highly ordered TiO₂ nanotube arrays, for example, in DSSC.¹³

Fig. 1c and 1d show the surface topologies of freestanding TiO₂ nanotube arrays at low and high magnification, respectively, after removal of the nanowires on the top. Highly ordered arrays of nanotubes are clearly evident. The average tube diameter *D*, wall thickness *w*, and interpore distance λ_{C-C} are 90 nm, 15 nm, and 120 nm, respectively. The cross-sectional SEM image shown in Fig. 1e confirms that the arrays of nanotubes were closely packed and oriented normal to the membrane surface, extending from one end to the other. The bottoms of the nanotubes were closed (Fig. 1e and 1f). The thickness of the freestanding membrane was ~135 μm after 60 h anodization, with the thickness able to be tuned by controlling anodization conditions. The nanotubular morphology of these vertically oriented arrays offers a large internal surface area with no concomitant decrease in geometric and structural order, making them excellent electron percolation pathways for vectorial charge transfer between interfaces.³⁸ This is in sharp contrast to the “electron-hopping” in a film of sintered TiO₂ nanoparticles, commonly used in DSSCs, where the random dispersion of nanoparticles in the sintered film leads to increased scattering of free electrons and electron trapping at the interfaces, thereby reducing electron mobility.

2. Crystalline evolution in TiO₂ nanotube arrays

In order to capitalize on the advantageous nanotubular structures of TiO₂ for a wide range of applications, *e.g.*, DSSCs and hydrogen generation, the as-prepared amorphous TiO₂ nanotube membrane should be transformed into the photoactive anatase or rutile phase.³² In this context, systematic Raman scattering measurements³⁹ on freestanding TiO₂ nanotube arrays annealed at different temperatures were carried out to monitor the high temperature annealing-induced crystalline phase formation. Each sample was scanned at least three times with the average intensity shown in Fig. 3. Amorphous TiO₂ had a broad spectrum ranging from 100 cm⁻¹ to 1000 cm⁻¹ (dotted curve in Fig. 3a). Annealing nanotubes at 200 °C did not induce the formation of the crystalline phase (solid curve in Fig. 3a where a broad spectrum was still observed). By contrast, anatase TiO₂ started to emerge when annealed at 300 °C, as evidenced by the specific peaks at 144 cm⁻¹, 399 cm⁻¹, 516 cm⁻¹, and 640 cm⁻¹ that can be assigned to the anatase phase (dashed curve in Fig. 3a);³⁴

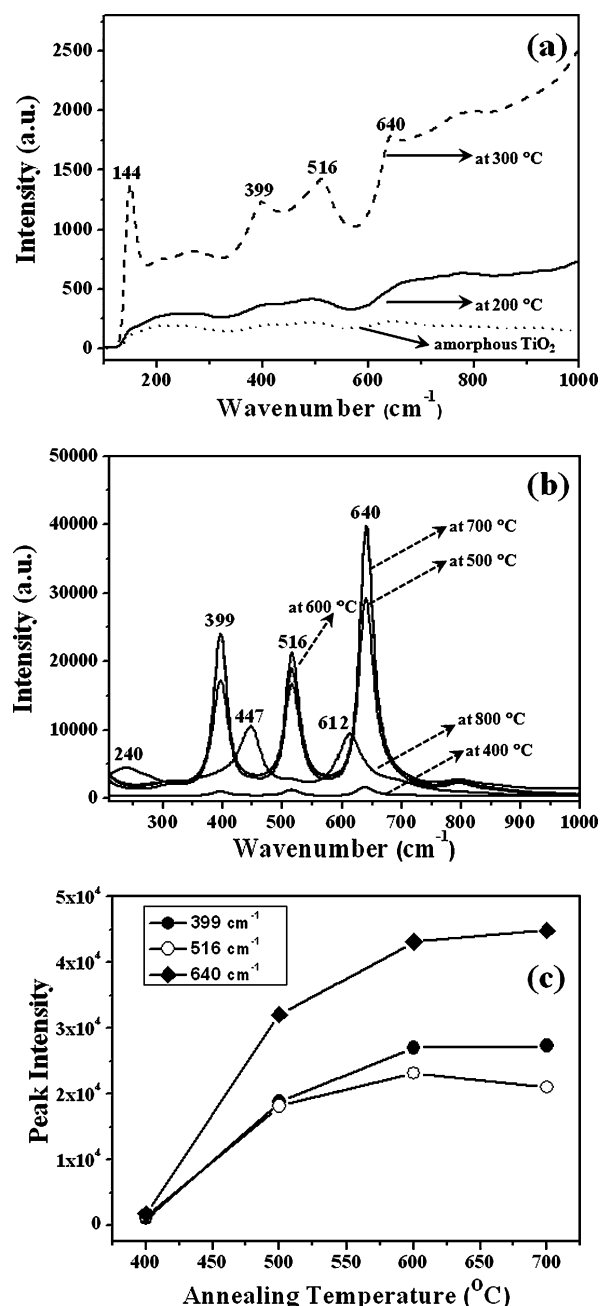


Fig. 3 (a–b): Raman spectra of TiO₂ nanotube arrays annealed at different temperatures. (c): Peak intensity as a function of annealing temperature at specific peak positions, *i.e.*, 399 cm⁻¹, 516 cm⁻¹, and 640 cm⁻¹ for the anatase TiO₂.

a strong background superimposed on the spectrum might be due to the co-existence of amorphous and crystalline TiO₂.

The Raman spectra of TiO₂ nanotubes annealed at temperatures higher than 400 °C are shown in Fig. 3b. As the annealing temperature increased, the Raman intensity increased and reached the maximum at 700 °C (Fig. 3b). The peak intensity at 399 cm⁻¹, 516 cm⁻¹, and 640 cm⁻¹ as a function of annealing temperature is summarized in Fig. 3c, clearly suggesting that when the annealing temperature was higher than 600 °C, the crystallization of nanotubes was complete, in other words,

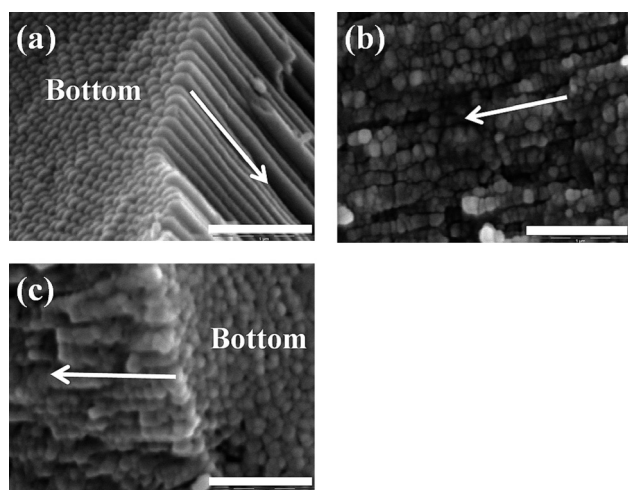


Fig. 4 SEM images of TiO₂ nanotubes annealed at high temperature. (a) 600 °C, (b) 700 °C and (c) 800 °C. The arrows indicate the direction that is perpendicular to the TiO₂ nanotube membrane. Scale bar = 1 μm.

complete transformation from amorphous TiO₂ to anatase TiO₂ was achieved at 600 °C. When the annealing temperature was higher than 700 °C, a transition from anatase to the rutile phase occurred. For the sample annealed at 800 °C, specific Raman peaks at 240 cm⁻¹, 447 cm⁻¹ and 612 cm⁻¹ can be assigned to rutile TiO₂ (Fig. 3b).^{40,41} It is noteworthy that the anatase to rutile transition temperature is much higher than the reported 620 °C value,³² where the TiO₂ nanotubes situated on Ti foil were used directly and Ti was found to promote the anatase to rutile transition. In the present study, however, freestanding TiO₂ nanotube arrays were used; there was no catalyzing effect from Ti on the crystalline transition. As a result, a higher transition temperature was observed. We also note that the nanotubular structures were retained with annealing temperatures up to 600 °C, which is in agreement with results in the literature.^{32,39} Further increase in annealing temperature (*e.g.*, 700 °C and 800 °C) led to the collapse of nanotubular structures; this can be attributed to the expansion of crystalline grains as shown in SEM images (Fig. 4).

3. Formation of TiO₂ nanoplates

To better understand the crystalline formation in freestanding TiO₂ nanotubes induced by high temperature annealing, ultramicrotoming was performed. Namely, TiO₂ nanotube arrays, after annealing at different temperatures, were embedded in Spurr's resin and thin sectioned (see Experimental section). Subsequently, they were imaged by TEM. In the control experiment, amorphous TiO₂ nanotube arrays exhibited a featureless selected area electron diffraction (SAED) pattern (inset in Fig. 5a) as expected. For the TiO₂ nanotube arrays annealed at 200 °C, the SAED pattern indicated that the nanotubes were still amorphous (inset in Fig. 5b). For the 300 °C annealed TiO₂ sample, the TEM image showed a majority of the nanotubular morphology (Fig. 5c), while the nanoplates can be seen in some locations. The SAED in the inset implied the crystalline formation in the nanotubes. Quite intriguingly, as the annealing temperature further increased to 400 °C and above, plate-like

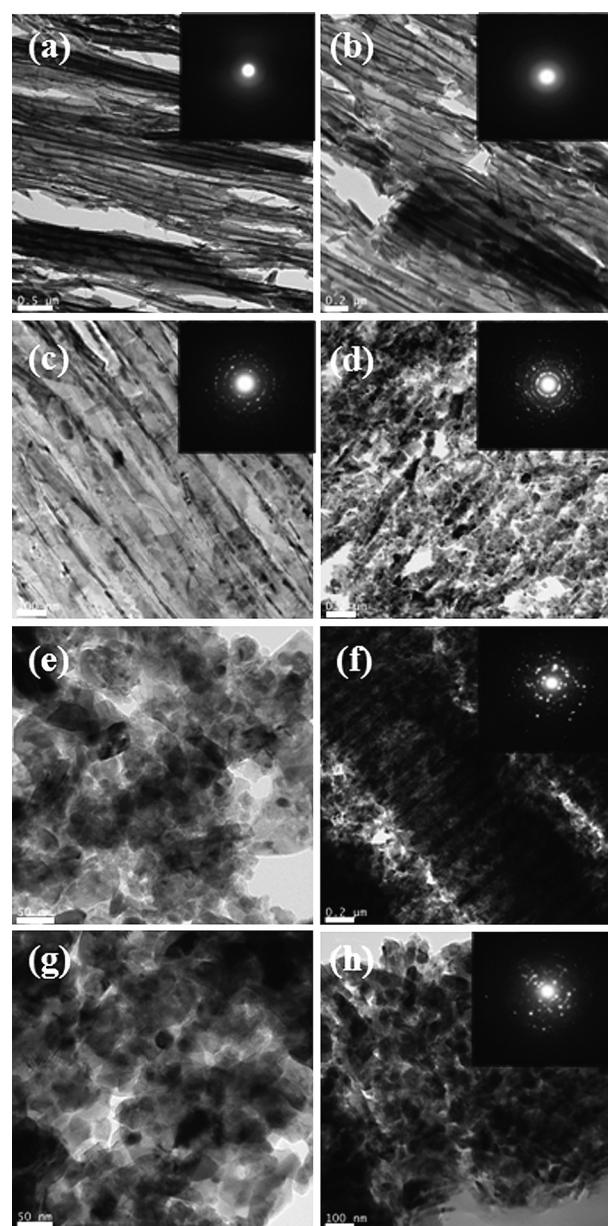


Fig. 5 TEM images of TiO₂ nanotube arrays annealed at different temperatures in air for 3 h. Ultra thin sections were obtained by microtoming the freestanding TiO₂ membrane embedded in Spurr's resin. (a) Amorphous TiO₂, scale bar = 500 nm; (b) TiO₂ annealed at 200 °C, scale bar = 200 nm; (c) TiO₂ annealed at 300 °C, scale bar = 100 nm; (d) low magnification (scale bar = 200 nm) and (e) high magnification (scale bar = 50 nm) TEM images of TiO₂ annealed at 400 °C; (f) low magnification (scale bar = 200 nm) and (g) high magnification (scale bar = 50 nm) TEM images of TiO₂ annealed at 500 °C; (h) TiO₂ annealed at 600 °C, scale bar = 100 nm. The corresponding selected area electron diffraction (SAED) patterns are shown in insets.

nanostructures became evident (Fig. 5d–h), with the SAED patterns shown in the insets clearly demonstrating the crystalline nature of these samples. The nanoplates were believed to be broken from the crystalline TiO₂ nanotube arrays (Fig. 5f and 6 in which nanoplates were seen to reside within the nanotube, packed along its long axis, and be about to disassemble from the nanotubes). The breakage was driven by the mechanical stress

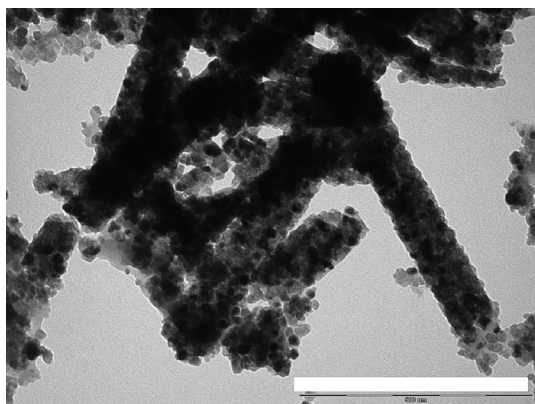
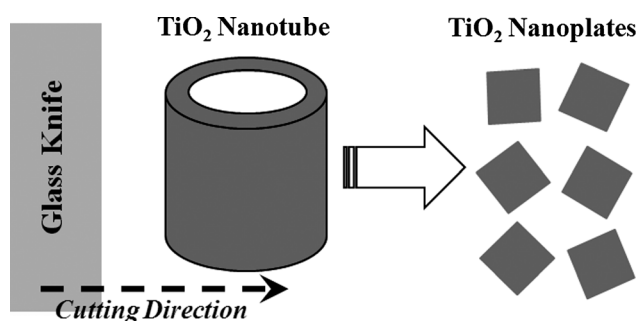


Fig. 6 TEM image of TiO₂ nanoplates obtained from ultramicrotoming TiO₂ nanotubes that were annealed at 500 °C, scale bar = 500 nm.



Scheme 1 Schematic illustration of the formation of TiO₂ nanoplates from nanotubes during ultramicrotoming crystalline TiO₂ nanotube arrays embedded in Spurr's resin.

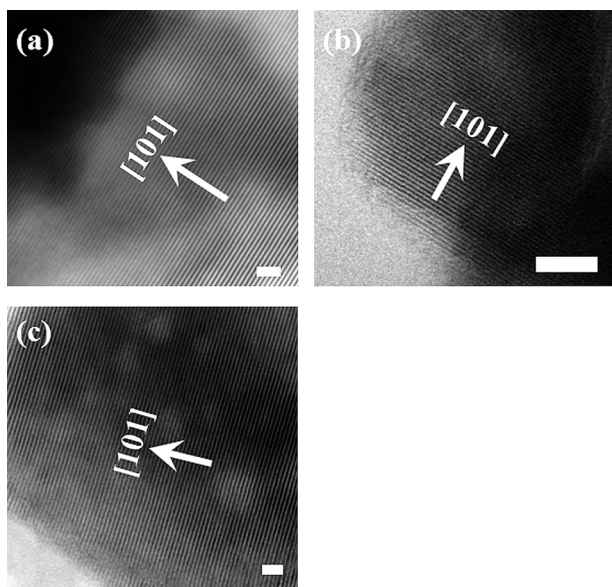


Fig. 7 HRTEM images of single crystalline TiO₂ nanoplates obtained from the ultramicrotoming of TiO₂ nanotubes. (a) Annealed at 400 °C, scale bar = 2 nm; (b) annealed at 500 °C, scale bar = 5 nm; (c) annealed at 600 °C, scale bar = 2 nm.

during microtoming using a freshly made glass knife. The formation mechanism of TiO₂ nanoplates from crystalline TiO₂ nanotube arrays is depicted in Scheme 1 in which the microtoming direction was perpendicular to the nanotube walls. The HRTEM images of single TiO₂ nanoplates from the samples annealed at different temperatures (*i.e.*, 400 °C, 500 °C, and 600 °C) are shown in Fig. 7, where all nanoplates possessed the [101] crystalline lattice, suggesting that they were single crystalline. Given the 50 nm lateral dimension (Fig. 6 and 7) and the 15 nm wall thickness (Fig. 1d), they are thin plate-like in shape.

On the basis of the Raman spectra of the TiO₂ nanotubes and the TEM results from microtomed thin sections (Fig. 3 and 5), the formation of crystalline TiO₂ nanotubes and the subsequent formation of nanoplates can be rationalized as follows. For the amorphous and low temperature annealed nanotubes, no specific Raman peaks of crystalline TiO₂ were observed (Fig. 3a), and no diffraction associated with the crystalline phase was seen (Fig. 5a–b), confirming that the nanotubes were amorphous. Higher temperature annealing induced crystal formation in the nanotube walls. With increased annealing temperature ($T \geq 300$ °C), the crystalline domain increased in size and reached the maximum that was dictated by the nanotube wall thickness, annealing temperature, and crystalline stability. At these temperatures, specific Raman peaks of anatase or rutile TiO₂ appeared (Fig. 3b), with the TiO₂ nanotube arrays maintaining their tubular morphology after annealing at temperatures up to 600 °C. When subjected to the ultramicrotome, the crystalline domains in the nanotube walls were broken and separated from one another (Scheme 1), thereby forming TiO₂ nanoplates as seen in the TEM images and the corresponding SAED patterns (Fig. 5d–h and 6).

Conclusions

In summary, we have reported the formation of TiO₂ nanowires, highly ordered TiO₂ nanotube arrays, and single crystalline TiO₂ nanoplates from electrochemically anodized Ti foil. Self organized, highly ordered TiO₂ nanotube arrays were fabricated by electrochemical anodization of Ti foil using fluorine-containing ethylene glycol as the electrolyte. Freestanding TiO₂ nanotube arrays can be readily obtained by mechanically detaching the formed membrane from the metallic Ti foil. Subsequently, TiO₂ nanowires formed in a “bamboo-splitting” fashion due to the electric field induced chemical etching of TiO₂ nanotubes can be isolated from the nanotubes buried underneath by mild ultrasonication in methanol. High temperature annealing transformed the as-prepared amorphous TiO₂ nanotube arrays into the anatase or rutile phase. The crystal formation in nanotubes as a function of annealing temperature was systematically explored by Raman spectroscopy and TEM measurements. Finally, ultramicrotoming annealed TiO₂ nanotube arrays broke the crystalline domains in the tube and yielded single crystalline TiO₂ nanoplates as revealed by HRTEM and corresponding SAED characterizations. To the best of our knowledge, this is the first report on disintegrating anodic TiO₂ nanotubes into single crystalline TiO₂ nanoplates. Based on these results, we envisage that high temperature annealed TiO₂ nanotube arrays could be transformed into nanoplates by strong mechanical forces, *e.g.*, milling or simply grinding. The present study not only

demonstrates a simple route to producing various TiO₂ nanostructures that may further extend the high performance applications of semiconductor TiO₂, but also provides valuable insights into the temperature dependent crystalline transformation in anodic TiO₂ nanotube arrays.

Acknowledgements

This work was supported by a 3M Non-tenured Faculty Award. Jun Wang thanks the Institute for Physical Research and Technology (IPRT) of Iowa State University for a Catron Fellowship. The authors also thank Tracy Pepper and Prof. Harry T. Horner at the Microscopy and NanoImaging Facility (MNIF) of Iowa State University for instructions on SEM and TEM characterization.

References

- 1 A. El Goresy, M. Chen, L. Dubrovinsky, P. Gillet and G. Graup, *Science*, 2001, **293**, 1467.
- 2 O. K. Varghese, D. W. Gong, M. Paulose, K. G. Ong, E. C. Dickey and C. A. Grimes, *Adv. Mater.*, 2003, **15**, 624.
- 3 G. K. Mor, M. A. Carvalho, O. K. Varghese, M. V. Pishko and C. A. Grimes, *J. Mater. Res.*, 2004, **19**, 628.
- 4 O. K. Varghese, D. Gong, M. Paulose, K. G. Ong and C. A. Grimes, *Sens. Actuators, B*, 2003, **93**, 338.
- 5 K. Shankar, G. K. Mor, A. Fitzgerald and C. A. Grimes, *J. Phys. Chem. C*, 2007, **111**, 21.
- 6 C. Ruan, M. Paulose, O. K. Varghese, G. K. Mor and C. A. Grimes, *J. Phys. Chem. B*, 2005, **109**, 15754.
- 7 J. M. Macak, M. Zlamal, J. Krysa and P. Schmuki, *Small*, 2007, **3**, 300.
- 8 S. P. Albu, A. Ghicov, J. M. Macak, R. Hahn and P. Schmuki, *Nano Lett.*, 2007, **7**, 1286.
- 9 J. Park, S. Bauer, K. von der Mark and P. Schmuki, *Nano Lett.*, 2007, **7**, 1686.
- 10 K. Shankar, G. K. Mor, H. E. Prakasam, O. K. Varghese and C. A. Grimes, *Langmuir*, 2007, **23**, 12445.
- 11 A. Kongkanand, K. Tvrđy, K. Takechi, M. Kuno and P. V. Kamat, *J. Am. Chem. Soc.*, 2008, **130**, 4007.
- 12 M. Paulose, K. Shankar, O. K. Varghese, G. K. Mor and C. A. Grimes, *J. Phys. D: Appl. Phys.*, 2006, **39**, 2498.
- 13 K. Zhu, T. B. Vinzant, N. R. Neale and A. J. Frank, *Nano Lett.*, 2007, **7**, 3739.
- 14 G. K. Mor, K. Shankar, M. Paulose, O. K. Varghese and C. A. Grimes, *Appl. Phys. Lett.*, 2007, **91**, 152111.
- 15 K. Shankar, G. K. Mor, H. E. Prakasam, S. Yoriya, M. Paulose, O. K. Varghese and C. A. Grimes, *Nanotechnology*, 2007, **18**, 065707.
- 16 G. K. Mor, K. Shankar, M. Paulose, O. K. Varghese and C. A. Grimes, *Nano Lett.*, 2006, **6**, 215.
- 17 K. Zhu, N. R. Neale, A. Miedaner and A. J. Frank, *Nano Lett.*, 2007, **7**, 69.
- 18 J. Wang, J. Xu, M. D. Goodman, Y. Chen, M. Cai, J. Shinar and Z. Q. Lin, *J. Mater. Chem.*, 2008, **18**, 3270.
- 19 B. O'Regan and M. Grätzel, *Nature*, 1991, **353**, 737.
- 20 J. Xu, J. Xia and Z. Q. Lin, *Angew. Chem., Int. Ed.*, 2007, **46**, 1860.
- 21 J. Xu, J. F. Xia, J. Wang, J. Shinar and Z. Q. Lin, *Appl. Phys. Lett.*, 2006, **89**, 133110.
- 22 D. Zimmitsky, C. Jiang, J. Xu, Z. Q. Lin and V. V. Tsukruk, *Langmuir*, 2007, **23**, 4509.
- 23 D. Zimmitsky, C. Jiang, J. Xu, Z. Q. Lin, L. Zhang and V. V. Tsukruk, *Langmuir*, 2007, **23**, 10176.
- 24 Z. Q. Lin, *Chem.-Eur. J.*, 2008, **14**, 6294.
- 25 J. Xu, J. Wang, M. Mitchell, P. Mukherjee, M. Jeffries-EL, J. W. Petrich and Z. Q. Lin, *J. Am. Chem. Soc.*, 2007, **129**, 12828.
- 26 M. D. Goodman, J. Xu, J. Wang and Z. Q. Lin, *Chem. Mater.*, 2009, **21**, 934.
- 27 I. Robel, V. Subramanian, M. Kuno and P. V. Kamat, *J. Am. Chem. Soc.*, 2006, **128**, 2385.
- 28 M. Grätzel, *Nature*, 2001, **414**, 338.
- 29 S. P. Albu, A. Ghicov, S. Aldabergenova, P. Drechsel, D. LeClere, G. E. Thompson, J. M. Macak and P. Schmuki, *Adv. Mater.*, 2008, **20**, 4135.
- 30 J. M. Macak, H. Tsuchiya, L. Taveira, S. Aldabergerova and P. Schmuki, *Angew. Chem., Int. Ed.*, 2005, **44**, 7463.
- 31 V. Likodimos, T. Stergiopoulos, P. Falaras, J. Kunze and P. Schmuki, *J. Phys. Chem. C*, 2008, **112**, 12687.
- 32 O. K. Varghese, D. W. Gong, M. Paulose, C. A. Grimes and E. C. Dickey, *J. Mater. Res.*, 2003, **18**, 156.
- 33 A. Ghicov, H. Tsuchiya, J. M. Macak and P. Schmuki, *Phys. Status Solidi A*, 2006, **203**, R28.
- 34 J. Wang and Z. Q. Lin, *Chem. Mater.*, 2008, **20**, 1257.
- 35 J. Wang and Z. Q. Lin, *J. Phys. Chem. C*, 2009, **113**, 4026.
- 36 J. H. Lim and J. Choi, *Small*, 2007, **3**, 1504.
- 37 A. L. Friedman, E. Panaitescu, C. Richter and L. Menon, *J. Nanosci. Nanotechnol.*, 2008, **8**, 5864.
- 38 C. A. Grimes, *J. Mater. Chem.*, 2007, **17**, 1451.
- 39 J. L. Zhao, X. H. Wang, T. Y. Sun and L. T. Li, *J. Alloys Compd.*, 2007, **434–435**, 792.
- 40 M. Aggour, T. H. Dittrich, A. Belaidi, I. Sieber and J. Rappich, *Phys. Status Solidi C*, 2005, **2**, 3344.
- 41 J. Zhao, X. Wang, R. Chen and L. Li, *Solid State Commun.*, 2005, **134**, 705.